

Radio observations of comet 9P/Tempel 1 with the Australia Telescope facilities during the Deep Impact encounter.

P. A. Jones^{1*}, J. M. Sarkissian¹, M. G. Burton², M. A. Voronkov^{1,3} and M. D. Filipović⁴

¹*Australia Telescope National Facility, PO Box 76, Epping NSW, 1710, Australia*

²*School of Physics, University of New South Wales, Sydney 2052, Australia*

³*Astro Space Centre, Profsoyuznaya st. 84/32, 117997 Moscow, Russia*

⁴*University of Western Sydney, Locked Bag 1797, Penrith South, DC, NSW 1797, Australia*

Accepted . Received ; in original form 2005 Nov 23

ABSTRACT

We present radio observations of comet 9P/Tempel 1 associated with the Deep Impact spacecraft collision of 2005 July 4. Weak 18-cm OH emission was detected with the Parkes 64-m telescope, in data averaged over July 4 to 6, at a level of 12 ± 3 mJy km/s, corresponding to OH production rate 2.8×10^{28} molecules/second (Despois et al. inversion model, or 1.0×10^{28} /s for the Schleicher & A’Hearn model). We did not detect the HCN 1-0 line with the Mopra 22-m telescope over the period July 2 to 6. The 3σ limit of 0.06 K km/s for HCN on July 4 after the impact gives the limit to the HCN production rate of $< 1.8 \times 10^{25}$ /s. We did not detect the HCN 1-0 line, 6.7 GHz CH₃OH line or 3.4-mm continuum with the Australia Telescope Compact Array (ATCA) on July 4, giving further limits on any small-scale structure due to an outburst. The 3σ limit on HCN emission of 2.5 K km/s from the ATCA around impact corresponds to limit $< 4 \times 10^{29}$ HCN molecules released by the impact.

Key words: comets:individual:9P/Tempel 1 - radio lines:Solar System

1 INTRODUCTION

The NASA mission “Deep Impact” encountered Comet 9P/Tempel 1 around 05:44 UT on 2005 July 4, with the high velocity collision of the impactor with the comet. The impactor had mass 370 kg and hit with a relative velocity of 10.2 km/s, so it was expected to excavate a hole to the depth of several tens of metres, and around 100 m in diameter. There was a coordinated international campaign of ground-based and satellite observations (Meech et al. 2005a, 2005b) to observe the impact event, to complement the observations from the flyby part of the Deep Impact mission, and to follow changes in the comet as new activity developed after the impact.

Comets are often described as “the most pristine material in the solar system” but the material we observe from the gas and dust in the coma has been chemically and physically processed by both solar heating and radiation. Even the surface of the nucleus has been modified from the original, presumably amorphous (Bar-Nun & Laufer 2003), ices. The dust and volatiles (similar to the icy grains in the ISM)

are processed to a surface crust, concurrent with the loss of volatiles, crystallisation and the formation of a dust mantle. One of the major aims of the Deep Impact mission was to study the ‘pristine’ material below the surface by exposing it in the crater formed by the impactor.

The major chemical constituents of comets are H₂O (which dissociates to OH), CO₂, CO and CH₃OH (methanol). Other important minor constituents, that can be observed at millimetre/submillimetre wavelengths are H₂CO (formaldehyde), CS, H₂S, HCN, HNC and CH₃CN. The relative abundances are found to vary considerably between different comets (Biver et al. 2002).

Comet 9P/Tempel 1 is a typical Jupiter-family periodic comet, chosen largely for its favourable orbit for the spacecraft encounter (A’Hearn et al. 2005a). At encounter, it was close to perihelion, with heliocentric distance 1.51 AU and geocentric distance 0.89 AU. The expected water release was 10^{28} molecules/second, before the effect of the impact (Lisse et al. 2005).

The spacecraft impact was a “successful” experiment releasing more than 10^6 kg of dust (Meech et al. 2005b), leading to changes monitored by the flyby spacecraft (A’Hearn

* E-mail:Paul.Jones@csiro.au

et al. 2005b) and the international campaign (Meech et al. 2005b) over a wide range of wavelengths and techniques.

2 OBSERVATIONS

The timing of the impact/flyby was chosen to allow simultaneous (redundant) NASA Deep Space Network (DSN) ground-station coverage from Goldstone (California) and Tidbinbilla (Australia). For the radio part of the international campaign, this meant Australia was geographically well-placed to monitor changes in the first few hours after impact on July 4. We made radio observations with the Parkes 64-m telescope to monitor OH, the Mopra 22-m telescope to monitor HCN (and CS) and the Australia Telescope Compact Array to detect any small-scale HCN, 3-mm continuum or 6.7 GHz CH₃OH maser.

2.1 Parkes OH observations

Parkes observations were made of the 1667.3590 and 1665.4018 MHz OH lines simultaneously, with frequency switching of the 8 MHz bandwidth between centre 1665.9 and 1666.9 MHz. The observations were made on 3 days, July 4, 5 and 6, with the on-source UT times and total integration time as given in Table 1. We used frequency switching (10 second period) rather than position switching for bandpass calibration, to maximise the on-source integration time. We used a correlator configuration with 8192 channels, giving 0.95 kHz or 0.176 km/s channels. The half-power beamwidth at 1.66 GHz was 14 arcmin. The comet was tracked using the proper motion from the ephemeris, updated every hour or so. The observing setup was checked by observations of the OH maser lines in evolved stars VY CMa, V Ant, R Crt and W Hya.

The data were reduced with the ATNF SPC package (<http://www.atnf.csiro.au/computing/software/spc.html>) which handles the RPFITS format output of the ATNF correlators, and allowed flexible, albeit labour intensive, processing of the buffers for the non-standard frequency-switched observations. The raw spectra had four quadrants, with spectra centred at both 1665.9 and 1666.9 MHz and two circular polarisations of the H-OH receiver. The bandpass correction was made by using the 1665.9 MHz data as signal, and the 1666.9 MHz data as reference in the signal-reference quotient, and the two polarisations were averaged. The data were folded (copied, shifted by the 1 MHz frequency shift, inverted and averaged) to combine the frequency shifted spectra. There were not regular standing waves in the spectra, but the baselines were still not very flat after the frequency switching calibration. The residual bandpass baseline was removed with a fifth-order polynomial. Separate spectra were extracted for the 1667.3590 and 1665.4018 MHz transitions, for each day of observation, corrected for different rest frequencies onto a geocentric velocity scale. The spectra were also shifted onto the velocity scale of the comet, using the geocentric velocity of the comet given in the JPL Horizons (<http://ssd.jpl.nasa.gov/horizons.html>) ephemeris (around 9 km/s).

2.2 Mopra HCN and CS observations

Mopra observations were made of the 88.63 GHz HCN 1 – 0 (hyperfine triplet 88630.4157, 88631.8473 and 88633.936 MHz) and 97.98095 GHz CS 2 – 1 lines, as given in Table 2 on five days, July 2 – 6. We used a correlator configuration with two linear polarisations each 32 MHz bandwidth and 1024 channels, giving 31 kHz or 0.106 km/s channels for HCN and 0.096 km/s for CS. Position switching mode was used to get good bandpass baseline. The halfpower beamwidth was 35 arcsec, and the comet was tracked using the positions from the JPL Horizons ephemeris. Pointing was checked with SiO masers after retuning the second polarisation. The pointing rms was around 9 arcsec, so this dominated over any residual errors in the ephemeris tracking. The combination of on-off switching, and pointing checks, meant that the on-source integration time was somewhat less than 50 percent of the observing time eg. 3.1 hours on July 4. The weather on July 2 – 4 was good for 3-mm observing, as shown by the T_{sys} in Table 2, with the before impact July 4 data at low elevation, but deteriorated on July 5 and 6 giving higher T_{sys} .

The data were also reduced with the ATNF SPC package, with the DFM (Data From Mopra) script (<http://www.phys.unsw.edu.au/astro/mopra/software.php>) used to automate the on-off position switching quotients and polarisation averaging. The spectra were combined for each day in geocentric velocity and also shifted onto the velocity scale of the comet, for fitting and combining different days.

2.3 ATCA HCN and continuum observations

Australia Telescope Compact Array (ATCA) observations of the HCN 1 – 0 line were made on July 4, using the H75 array. This array provided two-dimensional u,v - coverage for the observations near the equator, and short baselines. The array at 3-mm uses five (of the six) 22-m telescopes, with primary beam 35 arcsec. The correlator configuration was FULL_16.256-64 with the first IF having 16 MHz bandwidth and 256 channels each 62.5 kHz or 0.21 km/s and the second IF 64 MHz bandwidth and 64 channels for calibration and continuum observations. The phase and pointing centres were tracked using an ephemeris file generated from the JPL Horizons ephemeris. The strong 3-mm sources 0537-441 and 1253-055 (3C279) were used as setup sources and primary calibrators. The secondary, phase calibrator was 1334-127. The pointing was updated using 1334-127 every hour or so, and the system temperature measured every half hour.

The observations were reduced with the MIRIAD package (Sault, Teuben & Wright 1995; <http://www.atnf.csiro.au/computing/software/miriad/>) including the specific routines for 3-mm ATCA observations, such as corrections for system temperature, gain as a function of elevation and antenna position errors. The primary flux calibration used sources 0537-441, 1253-055 and 1830-211 and flux values from ATCA monitoring of strong, albeit, variable calibrators relative to the flux of the planets. We did not observe planetary flux calibrators during our run, as the planets were either resolved or not in the accessible right ascension range. The synthesised beam size is 6.7×4.8 arcsec² at position angle 112 deg.

2.4 ATCA CH₃OH observations

The antenna no. 6 of ATCA, which is not equipped with the 3-mm receiver, was used to observe the $5_1 - 6_0$ A⁺ methanol (CH₃OH) transition at 6668.5128 MHz simultaneously with the HCN 1-0 observations by the rest of the array on July 4. The broad band signal was fed into the Long Baseline Array data acquisition system (LBA DAS) configured to digitize 4 MHz of bandwidth. This digital signal was recorded on a computer hard disk using the capture card manufactured by the Metsähovi Radio Observatory (the VSIB card). The autocorrelation spectra were calculated off-line for each 10 seconds interval using the software supplied with the capture card. The mode used in software correlation split the 4 MHz bandwidth selected by DAS into 1024 spectral channels, providing a 0.18 km s^{-1} spectral resolution. Two orthogonal linear polarizations were recorded separately and averaged during the data processing. The pointing centre was updated once per hour (at 30 minutes of each UT hour) using the JPL Horizons ephemeris. At the given frequency the full width at half maximum of the beam was 7.2 arcmin. Although the antenna constantly tracked the comet, the hardware stopped recording periodically for a short period of time (probably to flush the buffers). This resulted in 10–30% loss of integration time.

The data processing was done using our own software. It included a weighted averaging to form 5 minute scans of data, a high-order polynomial baselining of each polarization for each scan, followed by the weighted averaging of individual polarizations and scans. Because the noise diode was not used in this non-standard setup, the rms in the spectrum was used as a measure of T_{sys} to calculate the weights of individual spectra for averaging. These weights appeared to stay almost the same (difference less than 0.1%) throughout the observations with the constant factor of about 1.8 between different polarizations. The flux scale was established by observing a test maser source G9.62-0.20E. This source exhibits periodic flares, with the date of our observations falling into a quiescent stage characterized by the flux density about 4700 Jy (Goedhart et al., 2003). The accuracy of the absolute flux density scale is determined by the “light curve” of Goedhart et al. (2003) and is about 10%. The radial velocity of this maser allowed it to be observed in the same 4 MHz band with the same setup of the conversion chain (local oscillators), as was used for the comet. Therefore, the maser was observed a few times to check the system and to test the conversion chain setup, which determines the relation between the spectral channels and frequencies.

3 RESULTS

3.1 Parkes OH results

The Parkes OH spectra were averaged over each of the three days of observations, and combined for the three days. A summary of the results is given in Table 1. We find no significant emission at the expected velocity (zero in our cometocentric velocity) for the 1667 or 1665 MHz OH lines on July 4 (the day of impact) or July 5 (one day after). We do find weak peaks for 1667 MHz line, but not the 1665 MHz line, on July 6 and the data for all three days combined. The spectrum of the 1667 MHz line for the three days combined

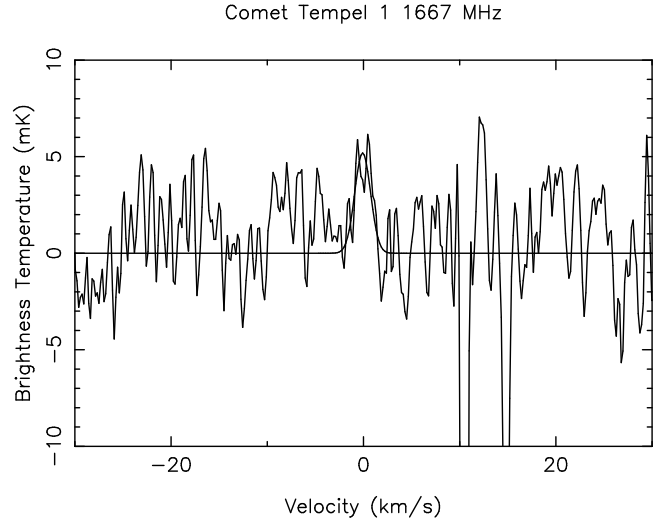


Figure 1. Spectrum of the OH 1667-MHz line in comet 9P/Tempel 1, integrated over 3 days of Parkes observations, 2005 July 4 – 6. The spectra have been combined after correcting for the geocentric velocity of the comet, so the velocity scale is relative to the comet ephemeris.

is shown in Fig. 1, with three point Hanning smoothing applied, and with the gaussian-line fit over-plotted.

There are some problems with the spectra. There are interference lines, that appear due to the frequency switching as positive peaks with two negative peaks half the intensity 1 MHz on either side. In Fig. 1, these appear as two strong negative features. Also, the spectral baselines are not quite flat, with some bumps, rather than simply thermal noise. This is perhaps not surprising, as with such long integrations (21.3 hours for all three days combined) we do find the RMS noise (Table 1) has decreased with the expected $t^{-1/2}$ to a factor 10^{-4} of the bandpass level ($T_{sys} \sim 27 \text{ K}$). It is quite a stringent requirement for the bandpass to be smooth to this 10^{-4} level, after frequency switch calibration.

The fitted emission in the 1667 MHz OH line integrated over the three days is peak $5.3 \pm 1.2 \text{ mK}$, velocity $0.0 \pm 0.2 \text{ km/s}$ and FWHM $2.0 \pm 0.6 \text{ km/s}$. Note that the uncertainty in the fitted peak, obtained with the fit in the SPC package, is smaller than the RMS of the individual (0.176 km/s) channels, since the line is resolved over many channels. We do consider the line significant at the 3σ level taking this into account. The fitted emission line for July 6 is $6.9 \pm 2.1 \text{ mK}$, velocity $-0.1 \pm 0.2 \text{ km/s}$ and FWHM $2.1 \pm 0.5 \text{ km/s}$.

The integrated flux density of the line is given in Table 1 (in mJy km/s) using the beam efficiency 0.7 and sensitivity 1.5 Jy/K from the Parkes RadioTelescope Users Guide. We also quote 3σ upper limits for the spectra without line detections, assuming limits to the fits for similar line width (2.0 km/s) as the weak detections. We use integrated flux in mJy rather than brightness in mK for the Parkes OH, as the scale of emission is smaller than the 14 arcmin beam.

We have also averaged the spectra for the 1665 and 1667 MHz lines, with the results shown in table 1. The 1665 and 1667 MHz OH lines have statistical weights 5 and 9 so this should slightly improve the signal to noise ratio. This does reduce the RMS noise, and we do detect the weak line at the expected velocity for the July 6 data and the data averaged

Table 1. Parkes 1667 and 1665 MHz OH results

Date	UT range	Int. time (hours)	Mean T_{sys} (K)	RMS T_a (mK)			Flux or 3σ limit (mJy km/s)			Q_{OH} (10^{28} /s)	N_{OH} (10^{34})
				1667	1665	mean	1667	1665	mean	1667	1667
Jul 4	04:55 – 12:50	7.39	26.4	4.4	4.9	3.3	< 12	< 14	< 9	< 3.0	< 1.3
Jul 5	05:09 – 12:54	5.95	26.6	6.5	6.0	4.3	< 18	< 17	< 12	< 4.3	< 2.0
Jul 6	04:50 – 12:55	7.96	26.9	5.1	5.3	3.7	16 ± 5	< 15	12 ± 3	3.9	1.7
Jul 4 – 6		21.3	26.7	3.1	3.2	2.3	12 ± 3	< 9	12 ± 3	2.8	1.3

over the three days. However, the gaussian fits to the lines are probably less robust than the fits to the 1667 MHz data, as there is a greater problem with interference lines in the combined 1667 and 1665 MHz data.

3.2 Mopra HCN and CS results

The Mopra HCN spectra were averaged over each of the five days of observations, except for the day of impact July 4, where the data were kept as before and after impact spectra. Since the observations were only of order 1 hour on-source integration time, except for July 4, we also combined data before impact for July 2 – 4, and after impact July 5 – 6. A summary of the results is given in Table 2. The CS was only observed at Mopra on July 3.

We did not detect either HCN or CS to quite low limits. The 3σ limits in Table 2 were calculated from the RMS T_a in the spectra, assuming nominal gaussian line half-power width 2.0 km/s. For HCN, to account for the three hyperfine components in the nominal 1:5:3 ratio, we can improve the signal to noise by shifting and averaging the two strongest hyperfine components and multiplying by (9/8). This gives an extra factor $(9/8)\sqrt{2} = 1.59$ in the limit (compared to factor $(9/5) = 1.8$ for simply taking the limit on the strongest hyperfine component and correcting for the extra weaker components). The limits are in T_{MB} , so there is a further factor of dividing by 0.49 for the main beam efficiency (Ladd et al. 2005).

3.3 ATCA HCN and continuum results

The ATCA HCN 1-0 and 3.4-mm continuum results are summarised in Table 3. We did not detect either the HCN in the line data cubes or the continuum emission. As well as combining all the data over the 8 hours of observations, we have broken up the ATCA data into roughly two-hour sections because we would expect compact (few arcsec) structure caused by the spacecraft impact to change over timescales of an hour or so. Two hours is about the shortest period that can be imaged with adequate u, v -coverage with the H75 array. The last two hour section has high noise, as the comet was getting low in the sky and data were lost from antenna shadowing of the shortest EW baselines.

The RMS in the continuum images and line data cubes are given in mJy/beam for the 6.7×4.8 arcsec² synthesised beam. The point source continuum flux limits can be taken as $3 \times$ RMS, for the nucleus. The dust cloud released by the impact should be a point source for the ATCA beam for several hours, given the dust velocity of 200 m/s reported

Table 4. ATCA CH₃OH $5_1 - 6_0$ A⁺ results

Date	UT range	Int. time (hours)	RMS (mJy)	3σ limit (mK km s ⁻¹)
Jul 4	05:45 – 13:14	5.94	180	< 4.2
Jul 4	05:45 – 07:30	1.32	360	< 8.9
Jul 4	07:30 – 09:30	1.60	340	< 9.4
Jul 4	09:30 – 11:14	1.40	350	< 8.0
Jul 4	11:14 – 13:14	1.62	350	< 8.5

by Meech et al. (2005b), and the velocity of larger particles seen in the millimetre wavelength is probably even less. The limit for the extended coma emission from the normal steady comet outflow is somewhat larger, with the expected r^{-2} dependence of dust density giving increasing flux when summed over larger and larger scales (eg. de Pater et al. 1998).

The spectral line limits were calculated, similar to the Mopra limits, assuming fitting errors for 2.0 km/s FWHM lines of the HCN triplet, and converted from mJy/beam to brightness temperature T_B with $T_B = (S/\Omega)(\lambda^2/2k)$ where Ω is beam solid angle.

3.4 ATCA CH₃OH results

The ATCA CH₃OH $5_1 - 6_0$ A⁺ results are summarized in Table 4. Similarly to the HCN 1-0 and 3.4-mm continuum results, in addition to combining all the data, four shorter (roughly two-hour) intervals have also been examined. We did not detect any methanol emission in either of these time intervals. The limits were calculated the same way as for Mopra data, assuming that 1 K of the main beam brightness temperature of a single ATCA antenna is equivalent to 6.8 Jy.

4 DISCUSSION

There was an extensive campaign of observations of comet 9P/Tempel 1 (Meech et al. 2005a, 2005b) associated with the Deep Impact mission, from the ground and spacecraft, over a wide range of wavebands. The results presented here will be most useful when combined with other complementary data into physical models. These data include (but are not restricted to) other 18-cm OH observations, from the Green Bank Telescope (GBT) and Nançay, and millimetre HCN, CS and CH₃OH observations from the IRAM-30m, CSO-10m and JCMT, including higher transitions. In the steady

Table 2. Mopra HCN 1-0 and CS 2-1 results. The HCN data are combined over each day of observation, except for the July 4 data which is averaged separately before and after the impact event. The data are further combined July 2 – 4 before impact and July 5 – 6 after impact, and all five days data.

Date	UT range	Int. time (hours)	Mean T_{sys} (K)	RMS T_a (mK)	3 σ limit (K km/s)	Q_{HCN} (10^{25} /s)	N_{HCN} (10^{30})
HCN							
Jul 2	08:24 – 10:54	1.17	209	17	< 0.11	< 3.3	< 0.6
Jul 3	07:20 – 12:52	1.00	185	15	< 0.10	< 2.8	< 0.5
Jul 4 before	03:58 – 05:54	0.57	246	29	< 0.20	< 5.7	< 1.1
Jul 4 after	06:10 – 13:28	2.57	190	9	< 0.06	< 1.8	< 0.3
Jul 5	04:09 – 06:40	0.83	243	22	< 0.15	< 4.4	< 0.8
Jul 6	04:26 – 07:11	0.88	272	24	< 0.16	< 4.7	< 0.9
Jul 2 – 4 before		2.73	204	10	< 0.07	< 1.9	< 0.4
Jul 5 – 6 after		1.72	257	15	< 0.10	< 3.0	< 0.6
Jul 2 – 6 all		7.02	206	6	< 0.04	< 1.1	< 0.2
CS							
Jul 3	08:37 – 09:51	0.50	163	20	< 0.08	-	-

Table 3. ATCA HCN 1-0 line and 3.4-mm continuum results.

Date	UT range	RMS line (mJy)	3 σ limit line (K km/s)	RMS continuum (mJy)	Q_{HCN} (10^{25} /s)	N_{HCN} (10^{30})
Jul 4	05:30 – 13:20	48	< 1.2	1.6	< 6	< 0.2
Jul 4	05:30 – 07:30	99	< 2.5	3.1	< 12	< 0.4
Jul 4	07:30 – 09:30	75	< 1.9	2.2	< 9	< 0.3
Jul 4	09:30 – 11:20	77	< 1.9	2.5	< 9	< 0.3
Jul 4	11:20 – 13:20	155	< 3.9	5.5	< 18	< 0.6

state, the models typically assume constant velocity outflow from the nucleus (which would give radial dependence of density $n(r) \propto r^{-2}$ and column density integrated along the line of sight $N(r) \propto r^{-1}$), modified by the time-dependent formation and destruction of the species of interest.

For lines such as HCN 1-0 the conversion between integrated line intensity and column density (and production rate) is relatively straight-forward, using standard radiative transfer equations (e.g. Crovisier et al. 1987), but for the 18-cm OH lines there is additional complexity (e.g. Crovisier et al. 2002) with UV-pumping dependent on the heliocentric velocity, leading to inversion or anti-inversion of the levels (Despois et al. 1981; Schleicher & A’Hearn 1988). Taking into account the variety of maser transitions and pumping regimes observed in the interstellar medium, the case of the methanol emission is likely to be even more complex.

4.1 Production rates and number of molecules

We present here rough estimates of molecule production rates, or number of molecules, from our observations.

For OH, we have used the conversion between observed line flux (in mJy km/s) and derived production rate (Q_{OH} in molecules/s) from the work of Crovisier et al. (2002) with Nançay, scaling for inversion factor, heliocentric distance, background brightness temperature and beam area. We quote Q_{OH} in Table 1 and also calculate the number of OH molecules (N_{OH}) within the Parkes beam (7 arcmin or

272 000 km radius). We used the inversion factor 0.03 appropriate for the Despois et al. (1981) model, but note that the model of Schleicher & A’Hearn (1998) has inversion factor 0.08, which would decrease the estimates of Q_{OH} and N_{OH} by the factor 3/8. Given the discrepancies between the models at this small inversion factors (near a zero crossing) around heliocentric velocities near zero, the estimates of Q_{OH} and N_{OH} are subject to quite a large systematic error.

From the Mopra HCN flux limits, we derived the limits on HCN production rate (Q_{HCN}) in Table 2, by scaling from the predicted flux for the IRAM 30-m from Meech et al. (2005a), for the different beamsizes, and corrected for the ratios of the different HCN levels as observed by Biver et al. (2005a). The limits on the number of HCN molecules within the Mopra 35 arcsec beam (radius 11 300 km) was calculated from the production rate, on the simple constant velocity outflow model.

We similarly derived limits on HCN production rates in Table 3 from the ATCA HCN flux limits, and limits on the number of HCN molecules within the ATCA beam (radius 1800 km).

Note that expressed in brightness temperature, the Mopra limits on HCN are much lower than the ATCA limits, as Mopra has a much larger beam solid angle Ω , and this corresponds to somewhat lower limits with Mopra on the HCN production rate. However, the ATCA results are sensitive to the small-scale structure that might have been expected

from the spacecraft impact causing an outburst. In limiting such an outburst, the most appropriate 3σ limit is probably $N_{\text{HCN}} < 4 \times 10^{29}$ molecules from the ATCA over the period 05:30 – 07:30 UT, since the compact structure would expand out of the ATCA beam over the period of an hour or so. Similar limits on N_{HCN} are obtained for the Mopra and ATCA data averaged over the time after impact on the day Jul 4, although when averaging over these longer times material released by the impact would leave the beam area.

For the radio continuum, we used the simple model of Jewitt & Matthews (1997) and the 3σ limit of 4.8 mJy for Jul 4. We assumed temperature 300 K, as the rough average of the measured temperature range 260 to 329 K (A’Hearn et al., 2005b), giving black-body cross-sectional area less than $1.2 \times 10^9 \text{ m}^2$, as the limit on the coma dust. The thermal emission from the nucleus would be much less, given the mean radius 3.0 km (A’Hearn et al., 2005b). To convert the cross-section to mass, we assumed from Jewitt & Matthews (1997) dust opacity $\kappa(\lambda) = \kappa(\lambda_o)(\lambda/\lambda_o)^{-\beta}$ with $\kappa(1 \text{ mm}) = 0.05 \text{ m}^2 \text{ kg}^{-1}$, and $\beta = 0.9$. This gave dust mass less than $7 \times 10^{10} \text{ kg}$ within the ATCA beam (radius around 1800 km). Assuming a dust velocity 200 m/s, from Meech et al. (2005b), the timescale for dust moving out of the beam is several hours, so this mass can be taken as a limit on the mass released by the spacecraft impact, or alternatively converted to a limit on the steady outflow of $8 \times 10^6 \text{ kg/s}$. These limits are not very restrictive. We also note that the opacity κ is not well known; for example, Altenhoff et al. (1999) argue for a value $\kappa(1 \text{ mm}) = 7.5 \text{ m}^2 \text{ kg}^{-1}$ which would decrease the dust mass limits by a factor 150.

4.2 Comparison with other results

Pre-impact 18-cm OH observations were made at Nançay by Crovisier et al. (2005a) and Arecibo by Howell et al. (2005) from 2005 March to June, when the line was in strong absorption with large negative inversion parameter i . The average spectrum over Mar. 20 to Apr. 14 from Nançay observations (Crovisier et al. 2005a) had area $12 \pm 2 \text{ mJy km/s}$, corresponding to OH production rate 0.4×10^{28} molecules/second. The OH production rate increased, as would be expected, as the comet approached perihelion. Schleicher & Barnes (2005) estimated 0.6×10^{28} molecules/second for June 9 from optical narrow-band photometry. Post-impact OH observations were also made at Nançay by Biver et al. (2005b) and the GBT by Howell et al. (2005). The GBT observations over the period July 4 to 11 showed variability with a mean integrated area of 18 mJy km/s for this period (Howell et al. 2005). This is in good agreement with our Parkes OH results (Table 1) of $12 \pm 3 \text{ mJy km/s}$ for the overlapping period July 4 – 6, given;

- a) the variability of water emission, as determined by the SWAS observations (see below) and
- b) the likelihood of extra OH line variability due to the conditions of excitation.

Our estimate of OH production rate over July 4 – 6 of $2.8 \times 10^{28} \text{ /s}$ with Despois et al. (1981) inversion factor, or $1.0 \times 10^{28} \text{ /s}$ with Schleicher & A’Hearn (1998) inversion factor, indicates some increase in the OH production rate in the few days after impact.

The water production rate from 9P/Tempel 1 around the date of impact was monitored in the 557 GHz line by

the SWAS (Bensch et al. 2005a, 2005b) and Odin (Biver et al. 2005b) satellites. The SWAS observations (Bensch et al. 2005b) show water production between 2005 June 5 and July 9 varying by a factor of three from 0.4×10^{28} to 1.3×10^{28} molecules/second, but no statistically significant increase following the impact. They found water production rate for the three days following impact was $(0.66 \pm 0.15) \times 10^{28}$ molecules/second, with a 3σ limit of 9×10^{32} molecules released in an outburst, and less than a factor of two increase in water production due to a new active area. Before the impact event, it was suggested that the crater could lead to a new focus for out-gassing which would persist (A’Hearn et al. 2005a), but this was not observed (Meech et al. 2005b).

Near infrared spectroscopy with the Keck-2 telescope by Mumma et al. (2005) indicated an increase in water production rate from 1.2×10^{28} molecules/second on June 3 and 1.0×10^{28} molecules/second on July 4 before impact to $(1.7, 1.7, 2.1, 2.0) \times 10^{28}$ molecules/second measured after impact on three short periods on July 4 and one on July 5.

Our results for production rates of OH (the daughter product of the water) are broadly consistent with these results, but there are probably some systematic differences in calculated production rates between the different techniques due to model assumptions.

From observations with the ESA Rosetta spacecraft, Küppers et al. (2005) derive a total water vapour output of 1.5×10^{32} molecules due to the impact. This is much less than our upper limit of $< 1.3 \times 10^{34}$ OH molecules within the Parkes beam on July 4. Küppers et al. derive a large dust/ice ratio of greater than one by mass, corresponding to a dust mass $> 5 \times 10^6 \text{ kg}$ released by the impact. Our limit on dust mass from the 3.4-mm radio continuum of $< 7 \times 10^{10} \text{ kg}$ in the ATCA beam is, as noted earlier, not very restrictive.

Pre-impact millimetre-wave observations of HCN and other molecules were made with the IRAM-30m telescope by Biver et al. (2005a) giving integrated intensity of the HCN 1 – 0 line of $0.031 \pm 0.004 \text{ K km/s}$ over May 4.8 to 9.0. These HCN observations showed periodic variability in HCN production rate over the range $(0.5 - 1.0) \times 10^{25}$ molecules/second with period 1.7 days associated with the nucleus rotation. They did not detect CS. Our 3σ limits to the HCN 1-0 from the Mopra observations (Table 2) combined over the July 2 – 6 period ($< 1.1 \times 10^{25} \text{ /s}$) are close to this level and our results for the few days post-impact ($< 1.8 \times 10^{25} \text{ /s}$ on July 4 and $< 3.0 \times 10^{25} \text{ /s}$ on July 5 – 6) rule out any post-impact increase greater than about a factor of two. Mumma et al. (2005) report HCN production rates $2.1 \times 10^{25} \text{ /s}$ before impact (June 3) and $3.6 \times 10^{25} \text{ /s}$ after impact (July 4), with constant HCN to H₂O ratio of 0.2 %. This indicates that the increase due to the impact was small. However, these rates from Mumma et al. are a factor of two higher than our limit for July 4, and the pre-impact level from Biver et al. (2005a), which may indicate systematic errors due to model assumptions in translating HCN line fluxes to production rates.

Our limit on the total HCN released by the impact (ATCA data over 05:30 to 07:30 UT) of $< 4 \times 10^{29}$ molecules is close to the value of 3×10^{29} molecules (0.2 % of water amount 1.5×10^{32}) from Mumma et al.

Methanol (CH₃OH) is quite abundant in comets (e.g., Crovisier et al., 2005b). Biver et al. (2005a) found a production rate of methanol in the comet 9P/Tempel 1 of about

$(1-2) \times 10^{26}$ molecules/second. However, most methanol transitions observed so far are seen in thermal emission in the interstellar medium. The $5_1 - 6_0$ A^+ transition observed in our study is the brightest known maser transition. It has a relatively low spontaneous decay rate (about $1.5 \times 10^{-9} \text{ s}^{-1}$ according to the Hamiltonian of Mekhtiev, Godfrey & Hougen (1999) and usually has to be inverted (i.e. be a maser) to produce a detectable emission. The physical conditions required for this inversion to happen are studied only for the range of parameters typical for star-forming regions, where such masers are found. It is worth noting, however, that Slysh (2004) has suggested a model for interstellar masers in this transition, which form in large comet-like objects orbiting protostars. Although, no quantitative simulations of such model has been reported, the non-detection reported in this paper rules it out for the conditions typical for the Solar System.

ACKNOWLEDGMENTS

We would like to thank several people for help with these non-standard observations: Mike Kesteven for modifications of the Mopra control system to allow proper motion tracking of the comet; John Reynolds and Brett Preisig for help with Parkes schedules, receiver and frequency-switching hardware; Bob Sault for help with the ATCA schedule files; David Brodrick and Mark Wieringa for help with the ATCA control software; and Steven Tingay and Craig West for help with the broad-band disk recorder setup. We would like also to thank Nicolas Biver for helpful discussion, and referee's comments. The Australia Telescope is funded by the Commonwealth of Australia for operation as a National Facility managed by CSIRO.

REFERENCES

- A'Hearn M. F., Belton M. J. S., Delamere A., Blume W. H., 2005a, SSRv, 117, 1
A'Hearn M. F. et al., 2005b, Sci, 310, 258
Altenhoff W. J., et al., 1999, A&A, 348, 1020
Bar-Nun A., Laufer D., 2003, Icar, 161, 157
Bensch F., Melnick G. J., Patten B. M., 2005a, IAUC, 8550, 2
Bensch F., Melnick G. J., Neufeld D. A., Harwit M., Snell R. L., Patten B. M., 2005b, IAUS, 231, 133
Biver N., et al., 2002, EM&P, 90, 323
Biver N., Bockelee-Morvan D., Colom P., Crovisier J., Lecacheux A., Paubert G., 2005a, IAUC, 8538, 1
Biver N., et al., 2005b, DPS, 37, 710
Crovisier J., 1987, A&AS, 68, 223
Crovisier J., Colom P., Gérard E., Bockelee-Morvan D., Bourgois G., 2002, A&A, 393, 1053
Crovisier J., Colom P., Biver N., Bockelee-Morvan D., Lecacheux A., 2005a, IAUC, 8512, 3
Crovisier J., et al., 2005b, DPS, 37, 646
de Pater I., Forster J. R., Wright M., Butler B. J., Palmer P., Veal J. M., A'Hearn M. F., Snyder L. E., 1998, AJ, 116, 987
Despois D., Gerard E., Crovisier J., Kazes I., 1981, A&A, 99, 320

- Goedhart S., Gaylard M. J., van der Walt D. J., 2003, MNRAS, 339, L33
Howell E. S., Lovell A. J., Butler B., Schloerb F. P., 2005, DPS, 37, 712
Jewitt D. C., Matthews H. E., 1997, AJ, 113, 1145
Küppers M., et al., 2005, Nature, 437, 987
Ladd N., Purcell C., Wong T., Robertson S., 2005, PASA, 22, 62
Lisse C. M., A'Hearn M. F., Farnham T. L., Groussin O., Meech K. J., Fink U., Schleicher D. G., 2005, SSRv, 117, 161
Meech K. J., A'Hearn M. F., Fernandez Y. R., Lisse C. M., Weaver H. A., Biver N., Woodney L.M., 2005a, SSRv, 117, 291
Meech K. J., et al. 2005b, Sci, 310, 265
Mekhtiev M. A., Godfrey P. D., Hougen J. T., 1999, J. Mol. Spectrosc., 194, 171
Mumma M.J., et al. 2005, Sci, 310, 270
Sault R. J., Teuben P. J., Wright M. C. H., 1995, ASPC, 77, 433
Schleicher D. G., A'Hearn M. F., 1988, ApJ, 331, 1058
Schleicher D., Barnes K., 2005, IAUC, 8546, 1
Slysh V., 2004, ASPC, 321, 221